Determination of the Ratio of Nonlinear Optical Tensor Components at Solid−Liquid Interfaces Using Transmission Second-Harmonic Generation (TSHG)

Jianwei Li, Gregory He,† and Zhi Xu*

Department of Chemistry and the Center for Molecular Electronics, University of Missouri−St. Louis, St. Louis, Missouri 63121

Received: October 18, 1996; In Final Form: February 13, 1997[⊗]

A new experimental method has been established for the accurate determination of the nonlinear optical susceptibility tensor ratios ($\chi^{(2)}_{ZZZ}/\chi^{(2)}_{ZYY}$ and $\chi^{(2)}_{XXZ}/\chi^{(2)}_{ZYY}$) of molecules at solid−liquid interfaces using transmission second-harmonic generation. Experiments have been carried out with Crystal Violet, Nile Blue, and D289 molecules at the CH_3CN/quartz interface. The results have shown the excellent agreement with the theory of nonlinear optics. It has been demonstrated in this paper that for different molecules the phase angles of these two tensor ratios are quite different. Both the absolute values and the phase angles of the two tensor ratios can be obtained from the intensity ratios $I^{2\omega}_{P\rightarrow P,T}/I^{2\omega}_{S\rightarrow P,T}$ and $I^{2\omega}_{45°\rightarrow S,T}/I^{2\omega}_{S\rightarrow P,T}$ obtained at different angles of incidence and different interfacial densities.

I. Introduction

Solid−liquid interfacial chemistry is a rich interdisciplinary field that encompasses physical chemistry, electrochemistry, analytical chemistry, and surface science. The related fundamental and technological subjects include surface self-assembly,[1−12] electrochemistry,[13−22] corrosion inhibition,[23−34] electrochemical deposition,[35−42] and separation science.[43−44] From a fundamental aspect, we would like to understand (1) the nature of the chemical bond formed at the interface, (2) the interaction energy of different chemical species with substrate surfaces, (3) the effect of electrochemical potential on the molecular orientation and interfacial concentration, and (4) the reaction kinetics and dynamics at the interface. From an experimental aspect, we would like to know how to modify the physical and chemical properties of the interface so that interfacial reactions can be facilitated in desired directions. Studies are currently being carried out in this laboratory to address the above issues.

Because of the physical nature of the liquid phase involved, nonlinear optical methods including sum-frequency generation (SFG) and second-harmonic generation (SHG) are most suitable for probing the chemical and physical processes at solid−liquid interfaces. First, these methods are exclusively sensitive to the interface: only atoms and molecules within ∼100 Å on each side of the interface can contribute to the signal.[45−50] Second, different chemical species can be detected selectively using laser excitations at different frequencies due to "resonance enhancement".[51−54] Third, these methods are nondestructive since the light intensity employed is far below the damage threshold of molecules at solid−liquid interfaces.[55] Both the adsorption isothermal and molecular orientation at the interface can be determined by these nonlinear optical methods.

To obtain the orientation of molecules at solid−liquid interfaces, the ratios of different nonlinear tensor components in the second electrical susceptibility tensor matrix $\{\chi^{(2)}_{IJK}\}$ must be determined.[56] However, this is not straightforward in many cases since the phase of SHG/SFG signal generated by the different tensor components could be different. In this paper, a systematic method has been established for the determination of the ratios of nonlinear tensor components at solid−liquid interfaces using transmission second-harmonic generation (TSHG). Experiments have been carried out with Crystal Violet, Nile Blue, and D289 molecules at the CH_3CN/quartz interface, and the results are in excellent agreement with the theory.

II. Theoretical Background

2.1. Harmonic Wave Generated by a Thin Layer of Molecules at Interfaces. The electrical field of the second-harmonic wave generated by a thin molecular layer at interfaces can be expressed by the following equations:[57]

$$E^{2\omega}_{S,T} = \frac{i2\pi d}{\epsilon_0 \lambda (n_{r,2\omega} \cos \alpha_{r,2\omega} + n_{t,2\omega} \cos \alpha_{t,2\omega})} P^{2\omega}_S \qquad (1)$$

$$E^{2\omega}_{P,T} = -i2\pi d \times \frac{\left[\frac{n_{r,2\omega}}{n_{m,2\omega}} \sin \alpha_{m,2\omega} \cos(\alpha_{m,\omega} + \gamma) - \cos \alpha_{r,2\omega} \sin(\alpha_{m,\omega} + \gamma)\right]}{\epsilon_0 \lambda (n_{t,2\omega} \cos \alpha_{r,2\omega} + n_{r,2\omega} \cos \alpha_{t,2\omega})} P^{2\omega}_P \qquad (2)$$

In eqs 1 and 2, the subscripts S and P denote the polarization directions of the second harmonic waves that are perpendicular and parallel to the plane of incidence, respectively, the subscript T refers to the transmitted second-harmonic waves, ϵ_0 is the dielectric constant of the vacuum, λ is the wavelength of the excitation light in the vacuum, $\alpha_{r,2\omega}$ is the angle of reflection of the second-harmonic wave, $\alpha_{t,2\omega}$ is the angle of refraction of the second-harmonic wave in the substrate, $\alpha_{m,2\omega}$ is the angle of refraction of the harmonic wave in the molecular layer, $\alpha_{m,\omega}$ is the angle of refraction of the fundamental excitation in the molecular layer, γ is the angle between the p-polarized nonlinear polarization ($P^{2\omega}_P$) and the transmission propagation direction of the fundamental wave in the thin layer, $n_{r,2\omega}$ is the refractive index of the incidence phase for the second-harmonic wave, $n_{t,2\omega}$ is the refractive index of the substrate for the second-harmonic wave, $n_{m,2\omega}$ is the refractive index of the molecular layer for the harmonic wave, and d is the thickness of the nonlinear molecular layer. Figure 1 shows the relations among

* Corresponding author.
† Current address: Argonne National Laboratory, Building 200, Room D-185, 9700 S. Cass Ave., Argonne, IL 60439.
⊗ Abstract published in *Advance ACS Abstracts,* April 15, 1997.

S1089-5647(96)03225-7 CCC: $14.00

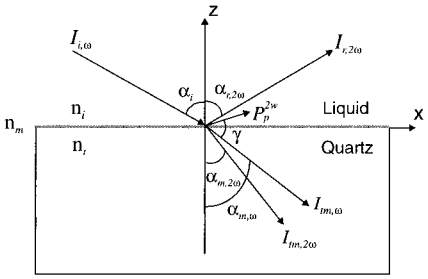

Figure 1. Schematic drawing of the propagation directions of the fundamental excitation ($I_{i,\omega}$), the transmitted fundamental excitation ($I_{tm,\omega}$), the reflected harmonic wave ($I_{r,2\omega}$), the transmitted harmonic wave ($I_{tm,2\omega}$), and the direction of the p-polarized nonlinear polarization ($P_P^{2\omega}$) at the liquid−quartz interface.

different physical quantities in which the $Z-X$ plane is the plane of incidence. According to Figure 1, eq 2 becomes

$$E_{P,T}^{2\omega} = \frac{i2\pi d\left[\frac{n_{r,2\omega}}{n_{m,2\omega}}\sin\alpha_{m,2\omega}P_Z^{2\omega} + \cos\alpha_{r,2\omega}P_X^{2\omega}\right]}{\epsilon_0\lambda(n_{t,2\omega}\cos\alpha_{r,2\omega} + n_{r,2\omega}\cos\alpha_{t,2\omega})} \quad (3)$$

For most solutions with low concentration, the refraction index of the second-harmonic generation in the incidence phase is very close to that of the fundamental excitation, i.e., $n_{r,2\omega} = n_{r,\omega}$. When fused silica is used as the substrate, the difference in refractive index between the fundamental excitation and the second-harmonic generation can be ignored.[58] Thus, from the principle of conservation of momentum in the tangential direction, the propagation directions of the second-harmonic wave in the incidence phase and the substrate should be identical to those of the fundamental excitation, i.e., $\alpha_{t,2\omega} \approx \alpha_t$ and $\alpha_{r,2\omega} \approx \alpha_i$, where α_i is the angle of incidence and α_t is the angle of refraction of the fundamental wave. Further, by applying Snell's law, $n_i \sin\alpha_i = n_t \sin\alpha_t = n_{m,2\omega}\sin\alpha_{m,2\omega}$, eqs 1 and 3 can be written as

$$E_{S,T}^{2\omega} = \frac{i2\pi d}{\epsilon_0\lambda(n_i\cos\alpha_i + n_t\cos\alpha_t)}P_S^{2\omega} \quad (4)$$

$$E_{P,T}^{2\omega} = \frac{i2\pi d\left[\frac{n_i^2}{(n_{m,2\omega})^2}\sin\alpha_i P_Z^{2\omega} + \cos\alpha_i P_X^{2\omega}\right]}{\epsilon_0\lambda(n_t\cos\alpha_i + n_i\cos\alpha_t)} \quad (5)$$

In eqs 4 and 5, n_i and n_t are the refractive indices of the liquid and solid phase for the fundamental excitation, respectively.

2.2. Nonlinear Tensor Components at Solid−Liquid Interfaces. For most solid−liquid interfaces, the interfacial layer is expected to have $C_{\infty v}$ symmetry. Under this condition, there are only seven nonzero tensor components in the nonlinear susceptibility tensor matrix $\{\chi_{IJK}^{(2)}\}$ and only three of them are independent:[56,59]

$$\chi_{ZZZ}^{(2)},\quad \chi_{ZXX}^{(2)} = \chi_{ZYY}^{(2)},\quad \chi_{XXZ}^{(2)} = \chi_{XZX}^{(2)} = \chi_{YYZ}^{(2)} = \chi_{YZY}^{(2)} \quad (6)$$

Further, for molecules in the thin layer, if $\beta_{z'z'z'}$ is the only dominant tensor component in the hyperpolarizibility tensor matrix $\{\beta_{ijk}^{(2)}\}$, the tensors in the above equations can be written as:[56]

$$\chi_{ZZZ}^{(2)} = N\beta_{z'z'z'}\langle\cos^3\theta\rangle$$

$$\chi_{ZXX}^{(2)} = \chi_{ZYY}^{(2)} = \chi_{XXZ}^{(2)} = \chi_{XZX}^{(2)} = \chi_{YYZ}^{(2)} = \chi_{YZY}^{(2)} = \frac{N}{2}\beta_{z'z'z'}\langle\cos\theta\sin^2\theta\rangle \quad (7)$$

where θ is the angle between the surface normal (Z) and the molecular coordinate (z'), and N is the interfacial density. If the ratio $\chi_{ZZZ}^{(2)}/\chi_{ZXX}^{(2)}$ can be determined from experiments and the orientation distribution is known, the average tilting angle θ can be obtained.

2.3. Surface Electric Field. The electric field experienced by molecules at the interface can be expressed as

$$E_Z = L_Z(\alpha_i)\,E_\omega(\alpha_i,\phi)\cos\phi\sin\alpha_i$$

$$E_X = L_X(\alpha_i)\,E_\omega(\alpha_i,\phi)\cos\phi\cos\alpha_i$$

$$E_Y = L_Y(\alpha_i)\,E_\omega(\alpha_i,\phi)\sin\phi \quad (8)$$

In the above equations $L_Z(\alpha_i)$, $L_X(\alpha_i)$, and $L_Y(\alpha_i)$ are the local field factors for electrical fields in the Z, X, and Y directions, respectively, α_i is the angle of incidence, ϕ is the polarization angle, i.e., the angle between the polarization direction of the electric field vector in the excitation beam and the plane of incidence, and $E_\omega(\alpha_i,\phi)$ is the electric field of the excitation beam at the interface. The three local field factors can be expressed as[60]

$$L_Y(\alpha_i) = (1 + r_S) = \frac{2n_i\cos\alpha_i}{(n_i\cos\alpha_i + n_t\cos\alpha_t)}$$

$$L_Z(\alpha_i) = (1 + r_p) = \frac{2n_t\cos\alpha_i}{(n_t\cos\alpha_i + n_i\cos\alpha_t)}$$

$$L_X(\alpha_i) = (1 - r_p) = \frac{2n_i\cos\alpha_t}{(n_t\cos\alpha_i + n_i\cos\alpha_t)} \quad (9)$$

In the above equations, r_S and r_P are the reflection coefficients for s- and p-polarized excitations, respectively.

2.4. s-Polarized SHG. For an interfacial layer with $C_{\infty v}$ symmetry, the nonlinear polarization in the Y direction can be expressed as the following:

$$P_Y^{2\omega} = \epsilon_0[\chi_{YYZ}^{(2)}E_YE_Z + \chi_{YZY}^{(2)}E_ZE_Y] = \epsilon_0\chi_{YYZ}^{(2)}[E_\omega(\alpha_i,\phi)]^2L_Y(\alpha_i)\,L_Z(\alpha_i)\sin(2\phi)\sin\alpha_i$$

Because $P_S^{2\omega} = P_Y^{2\omega}$, eq 4 becomes

$$E_{S,T}^{2\omega} = \frac{i2\pi dL_Y(\alpha_i)\,L_Z(\alpha_i)\,\chi_{YYZ}^{(2)}\sin(2\phi)\sin\alpha_i}{\lambda(n_i\cos\alpha_i + n_t\cos\alpha_t)}[E_\omega(\alpha_i,\phi)]^2 \quad (10)$$

The intensity of the s-polarized SHG light collected by the detector is[61]

$$I_{S,T}^{2\omega}(\alpha_i,\phi) = K_{S,T}(\alpha_i)(\sin 2\phi)^2[I_\omega(\alpha_i,\phi)]^2 \quad (11)$$

$$K_{S,T}(\alpha_i) = \frac{A_S^T(\alpha_i)(2\pi d)^2n_t\sin^2\alpha_i}{\epsilon_0c\lambda^2\epsilon_{r,i}}\left|\frac{L_Y(\alpha_i)\,L_Z(\alpha_i)\,\chi_{YYZ}^{(2)}}{n_t\cos\alpha_t + n_i\cos\alpha_i}\right|^2 \quad (12)$$

in which $A_S^T(\alpha_i)$ is the optical transmission of the entire detection system for the s-polarized harmonic wave after the interface, $\epsilon_{r,i}$ is the relative dielectric constant of the incidence phase for the fundamental excitation, and c is the speed of light in a vacuum.

2.5. Intensity Ratio of p-Polarized SHG. For an interfacial layer with $C_{\infty v}$ symmetry, the nonlinear polarization in the X and Z directions can be expressed as

$$P_X^{2\omega} = \epsilon_0[2L_X(\alpha_i)\, L_Z(\alpha_i)\chi_{XXZ}^{(2)} \sin\alpha_i \cos\alpha_i \cos^2\phi][E_\omega(\alpha_i,\phi)]^2 \quad (13)$$

$$P_Z^{2\omega} = \epsilon_0\{[L_Z{}^2(\alpha_i)\chi_{ZZZ}^{(2)} \sin^2\alpha_i + L_X{}^2(\alpha_i)\chi_{ZXX}^{(2)} \cos^2\alpha_i]\cos^2\phi + L_Y{}^2(\alpha_i)\chi_{ZYY}^{(2)} \sin^2\phi\}[E_\omega(\alpha_i,\phi)]^2 \quad (14)$$

The intensity of p-polarized SHG received by the detector is[61]

$$I_{P,T}^{2\omega}(\alpha_i,\phi) = \frac{A_P^T(\alpha_i)(2\pi d)^2 n_t c}{\epsilon_0 \lambda^2}\left|\frac{\dfrac{n_i{}^2}{(n_{m,2\omega})^2}\sin\alpha_i P_Z^{2\omega} - \cos\alpha_i P_X^{2\omega}}{(n_t\cos\alpha_i + n_i\cos\alpha_t)}\right|^2 \quad (15)$$

in which $A_P^T(\alpha_i)$ is the optical transmission of the entire detection system for the p-polarized harmonic wave after the interface.

A physical quantity that can be obtained easily is the ratio of the intensity of the p-polarized SHG signal excited by the p-polarized excitation ($\phi = 0°$) to that excited by the s-polarized excitation ($\phi = 90°$):

$$\left(\frac{I_{P\to P,T}^{2\omega}}{I_{S\to P,T}^{2\omega}}\right) = \left|\frac{P_Z^{2\omega}(\phi{=}0°)}{P_Z^{2\omega}(\phi{=}90°)} + \left(\frac{(n_{m,2\omega})^2\cos\alpha_i}{n_i{}^2\sin\alpha_i}\right)\frac{P_X^{2\omega}(\phi{=}0°)}{P_Z^{2\omega}(\phi{=}90°)}\right|^2 \quad (16)$$

Further, by using eqs 13 and 14, eq 16 can be written as

$$\left(\frac{I_{P\to P,T}^{2\omega}}{I_{S\to P,T}^{2\omega}}\right) = \left|\begin{aligned}&\frac{L_Z{}^2(\alpha_i)}{L_Y{}^2(\alpha_i)}\left(\frac{\chi_{ZZZ}^{(2)}}{\chi_{ZYY}^{(2)}}\right)\sin^2\alpha_i + \frac{L_X{}^2(\alpha_i)}{L_Y{}^2(\alpha_i)}\left(\frac{\chi_{ZXX}^{(2)}}{\chi_{ZYY}^{(2)}}\right)\cos^2\alpha_i\\ &+\frac{L_X(\alpha_i)\, L_Z(\alpha_i)}{L_Y{}^2(\alpha_i)}\left(\frac{(n_{m,2\omega})^2}{n_i{}^2}\right)\left(\frac{\chi_{XXZ}^{(2)}}{\chi_{ZYY}^{(2)}}\right)2\cos^2\alpha_i\end{aligned}\right|^2\left[\frac{I_P^\omega(\alpha_i)}{I_S^\omega(\alpha_i)}\right]^2 \quad (17)$$

Here, we define the intensity ratio $\rho(\alpha_i)$ as

$$\rho(\alpha_i) = \frac{\left(\dfrac{I_{P\to P,T}^{2\omega}}{I_{S\to P,T}^{2\omega}}\right)}{\left[\dfrac{I_P^\omega(\alpha_i)}{I_S^\omega(\alpha_i)}\right]^2} = \left|\begin{aligned}&\frac{L_Z{}^2(\alpha_i)}{L_Y{}^2(\alpha_i)}\left(\frac{\chi_{ZZZ}^{(2)}}{\chi_{ZYY}^{(2)}}\right)\sin^2\alpha_i + \frac{L_X{}^2(\alpha_i)}{L_Y{}^2(\alpha_i)}\left(\frac{\chi_{ZXX}^{(2)}}{\chi_{ZYY}^{(2)}}\right)\cos^2\alpha_i\\ &+\frac{L_X(\alpha_i)\, L_Z(\alpha_i)}{L_Z{}^2(\alpha_i)}\left(\frac{(n_{m,2\omega})^2}{n_i{}^2}\right)\left(\frac{\chi_{XXZ}^{(2)}}{\chi_{ZYY}^{(2)}}\right)2\cos^2\alpha_i\end{aligned}\right|^2 \quad (18)$$

Considering the fact that for an interfacial layer with $C_{\infty v}$ symmetry, $\chi_{ZXX}^{(2)} = \chi_{ZYY}^{(2)}$, eq 18 can be simplified:

$$\rho(\alpha_i) = \left|\frac{L_X{}^2(\alpha_i)}{L_Y{}^2(\alpha_i)}\cos^2\alpha_i + K_1\frac{L_Z{}^2(\alpha_i)}{L_Y{}^2(\alpha_i)}\sin^2\alpha_i + K_2\frac{L_X(\alpha_i)\, L_Z(\alpha_i)}{L_Y{}^2(\alpha_i)}2\cos^2\alpha_i\right|^2 \quad (19)$$

$$K_1 = \frac{\chi_{ZZZ}^{(2)}}{\chi_{ZYY}^{(2)}}, \quad K_2 = \left(\frac{(n_{m,2\omega})^2}{n_i{}^2}\right)\left(\frac{\chi_{XXZ}^{(2)}}{\chi_{ZYY}^{(2)}}\right) \quad (20)$$

2.6. Intensity of p-Polarized SHG. According to eqs 13−20, the intensity of p-polarized SHG can be expressed as

$$I_{P,T}^{2\omega}(\alpha_i,\phi) = K_{P,T}(\alpha_i)\left|\sin^2\phi + \left[\frac{L_X{}^2(\alpha_i)}{L_Y{}^2(\alpha_i)}\cos^2\alpha_i + K_1\frac{L_Z{}^2(\alpha_i)}{L_Y{}^2(\alpha_i)}\sin^2\alpha_i + K_2\frac{L_X(\alpha_i)\, L_Z(\alpha_i)}{L_Y{}^2(\alpha_i)}\cos^2\alpha_i\right]\cos^2\phi\right|^2[I_\omega(\alpha_i,\phi)]^2 \quad (21)$$

$$K_{P,T}(\alpha_i) = \frac{A_P^T(\alpha_i)(2\pi d)^2 n_t \sin^2\alpha_i}{\epsilon_0 c\lambda^2\epsilon_{r,i}}\left|\frac{L_Y{}^2(\alpha_i)\chi_{ZYY}^{(2)} n_i{}^2}{(n_t\cos\alpha_i + n_i\cos\alpha_t)\,(n_{m,2\omega})^2}\right|^2 \quad (22)$$

By comparing eq 19 with eq 21, one concludes[62,63]

$$I_{P,T}^{2\omega}(\alpha_i,\phi) = K_{P,T}(\alpha_i)\,|\sin^2\phi + e^{i\xi}\sqrt{\rho(\alpha_i)}\cos^2\phi|^2[I_\omega(\alpha_i,\phi)]^2 \quad (23)$$

The phase angle ξ can be determined by measuring the change of the p-polarized SHG signal as a function of the polarization angle ϕ.

2.7. Determination of Absolute value of K_2. The absolute value of K_2 can be determined from the ratio of the intensity of the s-polarized SHG signal generated by the excitation with the polarization angle of $\phi = 45°$ to that of the p-polarized SHG signal generated by the s-polarized excitation. According to eqs 11 and 23, this ratio can be expressed as

$$\left(\frac{I_{45°\to S,T}^{2\omega}}{I_{S\to P,T}^{2\omega}}\right) = \frac{A_S^T(\alpha_i)}{A_P^T(\alpha_i)}\left[\frac{I_\omega(\alpha_i,\phi{=}45°)}{I_\omega(\alpha_i,\phi{=}90°)}\right]^2\left|\frac{L_Z(\alpha_i)}{L_Y(\alpha_i)}\frac{K_2}{F(\alpha)}\right|^2 \quad (24)$$

$$F(\alpha) = \left[\frac{(n_i\cos\alpha_i + n_t\cos a_t)}{(n_t\cos\alpha_i + n_i\cos a_t)}\right] \quad (25)$$

$F(\alpha)$ can be calculated once the refractive indices of the liquid phase and the substrate are known. For most liquid/quartz interfaces, the value of $F(\alpha)$ changes from 1.00 to 1.01 when the angle of incidence is increased from 0° to 70°. As a result, the contribution of this factor can be ignored. Here we define another physical quantity η that can be obtained experimentally:

$$\eta = \left(\frac{I_{45°\to S,T}^{2\omega}}{I_{S\to P,T}^{2\omega}}\right)\frac{A_P^T(\alpha_i)}{A_S^T(\alpha_i)}\left[\frac{I_\omega(\alpha_i,\phi{=}90°)}{I_\omega(\alpha_i,\phi{=}45°)}\right]^2\left|\frac{L_Y(\alpha_i)}{L_Z(\alpha_i)}\right|^2 \quad (26)$$

The value of $|K_2|$ can then be determined from the following equation:

$$|K_2| \approx \sqrt{\eta} \quad (27)$$

When the interfacial concentration of nonlinear active molecules is low, their contribution to the refractive index can be ignored and one can assume $n_{m,2\omega} \approx n_i$. Thus, at low interfacial density limit we have $|K_2| = |\chi_{XXZ}^{(2)}/\chi_{ZYY}^{(2)}|$. If $\beta_{z'z'z'}$ is the only dominant

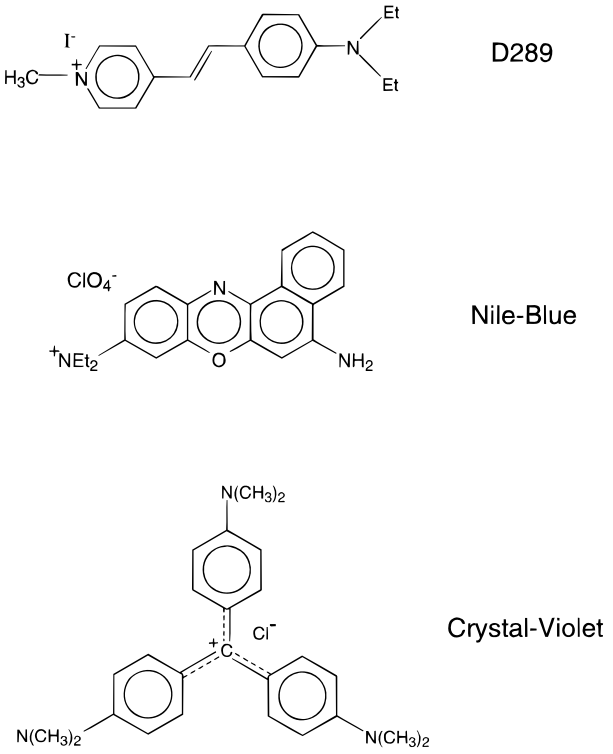

Figure 2. Molecular structures of D289, Nile Blue, and Crystal Violet.

tensor component in the hyperpolarizibility tensor matrix $\{\beta^{(2)}_{ijk}\}$, $|K_2| \approx 1$ according to eq 7.

2.8. Determination of K_1. After the phase angle ξ is known, the value of K_1 can be obtained from the values of the intensity ratio $\rho(\alpha_i)$ obtained at different angles of incidence according to the following equation:[64]

$$e^{i\xi}\sqrt{\rho(\alpha_i)} = \frac{L_X^2(\alpha_i)}{L_Y^2(\alpha_i)}\cos^2\alpha_i + e^{i\xi}|K_1|\frac{L_Z^2(\alpha_i)}{L_Y^2(\alpha_i)}\sin^2\alpha_i + e^{i\varphi}|K_2|\frac{L_X(\alpha_i)\,L_Z(\alpha_i)}{L_Y^2(\alpha_i)}2\cos^2\alpha_i \quad (28)$$

in which ζ and φ are the phase angles of the two tensor ratios K_1 and K_2, respectively. When the angle of incidence approaches zero, eq 28 is reduced to

$$e^{i\xi}\sqrt{\rho(0°)} = 1 + \frac{2n_t}{n_i}e^{i\varphi}|K_2| \quad (29)$$

From eq 29, both the phase angle φ and the value of $|K_2|$ can be obtained. Equation 29 provides an independent way for obtaining $|K_2|$. It is important to note that the phase angle ξ for the term $e^{i\xi}\sqrt{\rho(\alpha_i)}$ at each angle of incidence should be determined independently.

If $\beta_{z'z'z'}$ is the only dominant tensor component in the hyperpolarizibility tensor matrix $\{\beta^{(2)}_{ijk}\}$, the orientation factor $\langle\cos\theta\rangle/\langle\cos^3\theta\rangle$ can be determined according to the following equation:[65]

$$\frac{\langle\cos\theta\rangle}{\langle\cos^3\theta\rangle} = 1 + \frac{2}{|K_1|} \quad (30)$$

III. Experimental Section

3.1. Chemicals. Crystal Violet and Nile Blue were purchased from Aldrich. 4-(4-(Diethylamino)styryl)-*N*-methylpyridinium iodide, D289, was purchased from Molecular Probes. Figure 2 shows their molecular structures. The solution of each compound was prepared by dissolving the compound into HPLC-grade acetonitrile (CH_3CN). All three molecules have quite large molar absorptivity at 532 nm, $\epsilon = 13\,500\ M^{-1}\ cm^{-1}$ for D289, $\epsilon = 10\,700\ M^{-1}\ cm^{-1}$ for Nile Blue, and $\epsilon = 54\,800\ M^{-1}\ cm^{-1}$ for Crystal Violet. As a result, the SHG signal at 532 nm is resonantly enhanced and the contribution from the solvent and substrate can be ignored. In our experiments, the SHG signal from the dye molecules at the interface is typically more than 200 times stronger than the background SHG signal from the solvent and electrolyte molecules at the interface. The high concentration also ensures that the second-harmonic generation produced at the first solid−liquid interface will be absorbed completely by the dye molecules in the solution so that it will not have an interference effect with the SHG signal produced at the second solid−liquid interface.[66,67] A well-known electrolyte, tetrabutylammonium tetrafluoroborate ($TBABF_4$, Fisher), was added into the solutions of D289 and Crystal Violet to the concentration of 50 mM. For the Nile Blue solution, the concentration of the electrolyte was 5 mM.

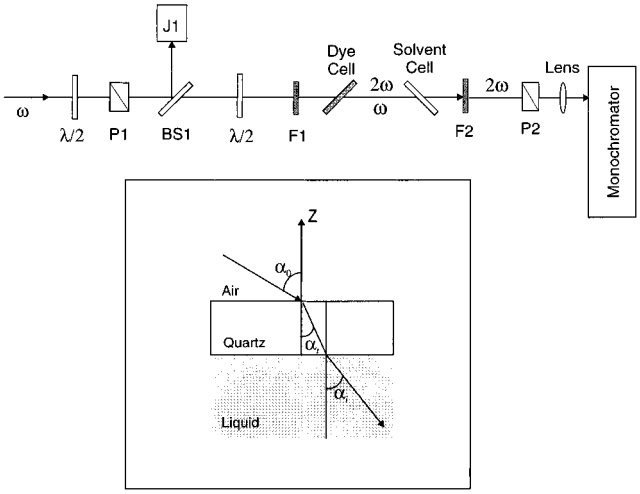

Figure 3. Optical layout of the SHG excitation-detection system. The inset shows the angle of incidence at the air/quartz interface (α_0), the angle of transmission in quartz (α_t), and the angle of incidence at the liquid/quartz interface (α_i).

3.2. Optical System. Figure 3 shows the optical layout of the SHG excitation-detection system. The laser excitation at 1064 nm was obtained from a Q-switched Nd:YAG laser (Spectra-Physics, GCR-170). The beam diameter was about 5 mm. The polarization and intensity of the excitation beam were controlled by a pair of $\lambda/2$ plates and a Glan-Laser polarizer with an extinction ratio of 100 000:1. The power density at the interface was kept below 100 MW/cm^2 to avoid the possible photon damage to the molecules. A beam splitter is placed between the polarizer and the second $\lambda/2$ plate to reflect ~1.3% of the pulse energy to the energy detector J1. F1 is a long pass filter to remove any 532 nm light generated by the optical components before the filter.

The fused silica dye cell was purchased from Starna Cell, Inc., which has an internal dimension of 10 × 40 × 45 mm. An identical optical cell containing HPLC-grade CH_3CN was placed in the beam pass to compensate the beam shift caused by the dye cell. Before the SHG measurement, the dye cell was cleaned in a hot sulfuric acid bath (~70 °C) for 60 min, and then it was rinsed thoroughly with deionized water. The surface was completely hydrophilic after the treatment. This was followed by rinsing the dye cell with Millipore water (18 MΩ cm) and HPLC-grade acetone and dried with nitrogen gas. The inset in Figure 3 shows the relations among different angles of incidence. The angle of incidence at the air/quartz interface, α_0, is related to the angle of incidence at the liquid/quartz interface, α_i, by Snell's law: $n_{air}\sin\alpha_0 = n_{liquid}\sin\alpha_i$.

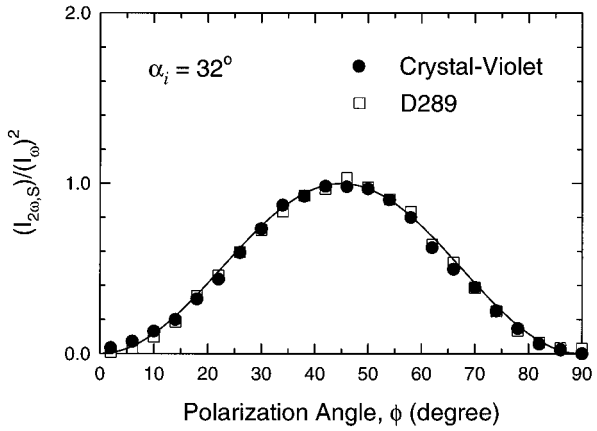

Figure 4. Dependence of the intensity ratio $I_S^{2\omega}(\alpha_i,\phi)/[I_\omega(\alpha_i,\phi)]^2$ on the polarization angle ϕ for D289 and Crystal Violet at the CH_3CN/quartz interface. The concentration of D289 was 8 mM and that of Crystal Violet was 4 mM. The solid curve is a fit using the function $(\sin 2\phi)^2$.

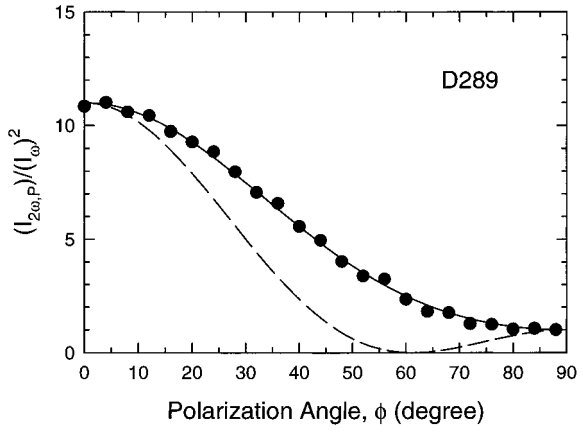

Figure 5. Change of the intensity ratio $I_P^{2\omega}(\alpha_i,\phi)/[I_\omega(\alpha_i,\phi)]^2$ as a function of the polarization angle ϕ for D289 at the CH_3CN/quartz interface. The concentration of D289 was 8 mM.

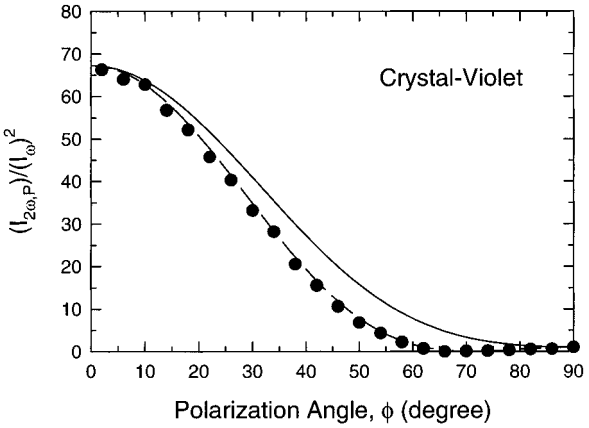

Figure 6. Intensity ratio $I_P^{2\omega}(\alpha_i,\phi)/[I_\omega(\alpha_i,\phi)]^2$ vs the polarization angle ϕ for Crystal Violet at the CH_3CN/quartz interface. The concentration of Crystal Violet was 4 mM.

The detection of the SHG signal at 532 nm was quite straightforward since the SHG signal propagates in the same direction of the excitation beam. As shown in Figure 3, a 532 nm band pass filter F2 was placed after the cell combination to reject the 1064 nm excitation light and to pass SHG at 532 nm. A dichroic sheet polarizer (P2) with an excitation ratio of 10 000:1 was placed in front of the monochromator to select the proper polarization for the SHG signal at 532 nm. The SHG signal was collected with a PMT, analyzed with a boxcar averager, and recorded with a computer.

3.3. Excitation Light Intensity at the Interface. Because of the reflection at the air/quartz interface of the dye cell, the light intensity at the second liquid/quartz interface is a function of both the polarization angle ϕ and the angle of incidence at the air/quartz interface, α_0. The reflection loss at the first quartz/liquid interface can be ignored since the refractive index of quartz (1.46) is very close to that of acetonitrile (1.34). Then, the excitation light intensity at the second solid−liquid interface is

$$I_\omega(\alpha_i,\phi) = [T_P(\alpha_0)\cos^2\phi + T_S(\alpha_0)\sin^2\phi]I_{\omega,0} \quad (31)$$

In eq 31, $I_{\omega,0}$ is the light intensity at the first air/quartz interface of the dye cell; $T_P(\alpha_0)$ and $T_S(\alpha_0)$ are the transmissivities of the air/quartz interface for p- and s-polarized excitations, respectively.

3.4. Optical Transmission Factor $A_S^T(\alpha_i)$ and $A_P^T(\alpha_i)$. For the optical components with their surface perpendicular to the propagation direction of the SHG wave, the reflection losses are identical for both s- and p-polarized SHG waves. Thus, we can write the two coefficients as

$$A_P^T(\alpha_i) = KA_P{T_P}^3(\alpha_0), \quad A_S^T(\alpha_i) = KA_S{T_S}^3(\alpha_0) \quad (32)$$

in which K is a constant, A_P and A_S are the optical transmissivities of the monochromator for p- and s-polarized lights, respectively, and ${T_P}^3(\alpha_0)$ and ${T_S}^3(\alpha_0)$ are used to account for the three reflection losses by the three air/quartz interfaces after the second liquid−quartz interface of the dye cell. For our detection system, $A_P/A_S \approx 1.85$ at 532 nm.

IV. Results and Discussion

4.1. s-Polarized SHG vs Polarization Angle ϕ. Figure 4 shows the change of the intensity ratio $I_{S,T}^{2\omega}(\alpha_i,\phi)/[I_\omega(\alpha_i,\phi)]^2$ as a function of the polarization angle ϕ for both Crystal Violet and D289 at the CH_3CN/quartz interface. The concentration of Crystal Violet was 4 mM and that of D289 was 8 mM. The angle of incidence at the CH_3CN/quartz interface was 32°. The solid line is calculated using the function $(\sin 2\phi)^2$, and the SHG responses of the two molecules have been normalized at ϕ = 45°. Figure 4 shows the excellent agreement of the experimental results with eq 11. Similar results have been obtained at different angles of incidence for all three molecules.

4.2. p-Polarized SHG vs Polarization Angle ϕ. Figure 5 shows the change of the intensity ratio $I_{P,T}^{2\omega}(\alpha_i,\phi)/[I_\omega(\alpha_i,\phi)]^2$ as a function of the polarization angle ϕ for D289 at the CH_3CN/quartz interface. The angle of incidence at the CH_3CN/quartz interface was 32°. As shown in Figure 5, the intensity ratio $\rho(\alpha_i)$ is about 11. The solid curve is calculated using the function $[\sin^2\phi + e^{i0}\sqrt{\rho_{D289}(\alpha_i)}\cos^2\phi]^2$, and the dashed curve is calculated using the function $[\sin^2\phi + e^{i\pi}\sqrt{\rho_{D289}(\alpha_i)}\cos^2\phi]^2$, according to eq 23. The excellent agreement of the experimental data with the solid curve indicates that, for D289, $e^{i0}\sqrt{\rho_{D289}(\alpha_i)}$ must be used in further calculations to obtain K_1. Nile Blue shows similar behavior.

Figure 6 shows the change of the intensity ratio $I_{P,T}^{2\omega}(\alpha_i,\phi)/[I_\omega(\alpha_i,\phi)]^2$ as a function of the polarization angle ϕ for Crystal Violet at the CH_3CN/quartz interface. The angle of incidence at the CH_3CN/quartz interface was 32°. The intensity ratio $\rho(\alpha_i)$ is about 67. The solid curve is calculated using the function $[\sin^2\phi + e^{i0}\sqrt{\rho_{D289}(\alpha_i)}\cos^2\phi]^2$, and the dashed curve is calculated using the function $[\sin^2\phi + e^{i\pi}\sqrt{\rho_{D289}(\alpha_i)}\cos^2\phi]^2$, according to eq 23. In contrast to D289, the experimental results agree well with the theoretical values calculated from the function $[\sin^2\phi +$

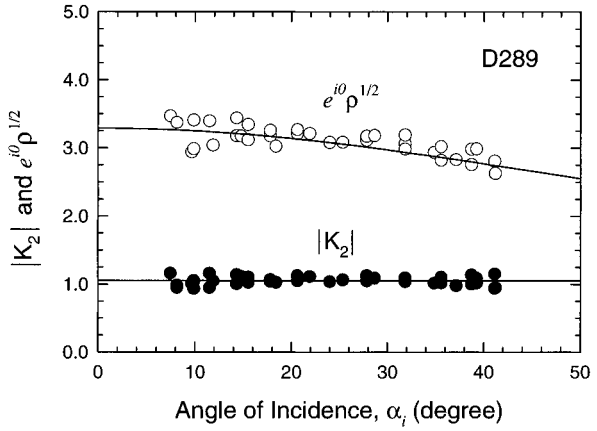

Figure 7. Change of $e^{i0}\sqrt{\rho}$ and $|K_2|$ as a function of the angle of incidence for D289 at the CH_3CN/quartz interface. The concentration of D289 was 8 mM.

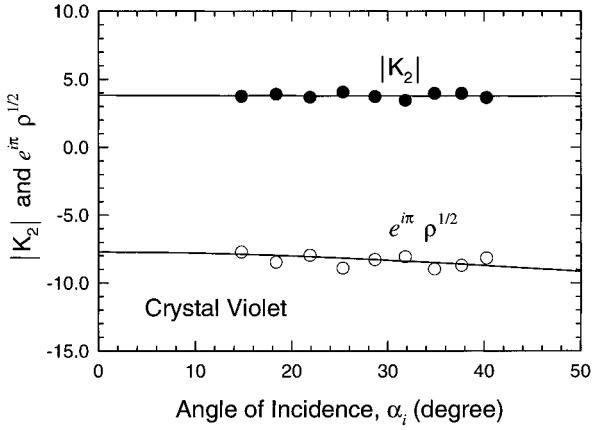

Figure 8. Change of $e^{i\pi}\sqrt{\rho}$ and $|K_2|$ as a function of the angle of incidence for Crystal Violet at the CH_3CN/quartz interface. The concentration of Crystal Violet was 4 mM. The angle of incidence was 32°.

$e^{i\pi}\sqrt{\rho_{C-Violet}(\alpha_i)}\cos^2\phi]^2$, indicating that for Crystal Violet $e^{i\pi}\sqrt{\rho_{C-Violet}(\alpha_i)}$ must be used in further calculations to obtain K_1. As shown in Figure 6, the intensity of the p-polarized SHG signal vanishes at the angle $\phi_0 = \arctan(\rho^{1/4}) \approx 71°$.

4.3. Determination of K_1 and K_2. Figure 7 shows the change of $e^{i0}\sqrt{\rho(\alpha_i)}$ as a function the angle of incidence for D289 at the CH_3CN/quartz interface (open circles). At all angles of incidence, the phase angle ξ remains unchanged, $\xi = 0$. The solid curve passing through the open circles is a theoretical fit according to eq 28, which generates the fitting parameters $|K_1| = 1.41$, $|K_2| = 1.06$, $\zeta = 0$, and $\varphi = 0$. Figure 7 also shows the values of $|K_2|$ obtained at different angles of incidence for D289 at the CH_3CN/quartz interface (filled circles). The values of $|K_2|$ were obtained according to eq 27. It is clear from Figure 7 that $|K_2|$ does not change with the angle of incidence, in agreement with eq 20. The average value of $|K_2|$ is 1.04. This value is very close to that obtained from the theoretical fitting for $e^{i0}\sqrt{\rho(\alpha_i)}$ as discussed above.

Figure 8 shows the change of $e^{i\pi}\sqrt{\rho(\alpha_i)}$ (open circles) and $|K_2|$ (filled circles) as a function of the angle of incidence for Crystal Violet at the CH_3CN/quartz interface. At all angles of incidence, the phase angle ξ remains unchanged, $\xi = \pi$. The solid line passing through the data points of $e^{i\pi}\sqrt{\rho(\alpha_i)}$ is a fit according to eq 28, which generates the fitting parameters $|K_1| = 7.9$, $|K_2| = 4.0$, $\zeta = \pi$, and $\varphi = \pi$. Similar to D289, the value of $|K_2|$ obtained according to eq 27 is independent of the angle of incidence. The average $|K_2|$ value is 3.9 for Crystal Violet.

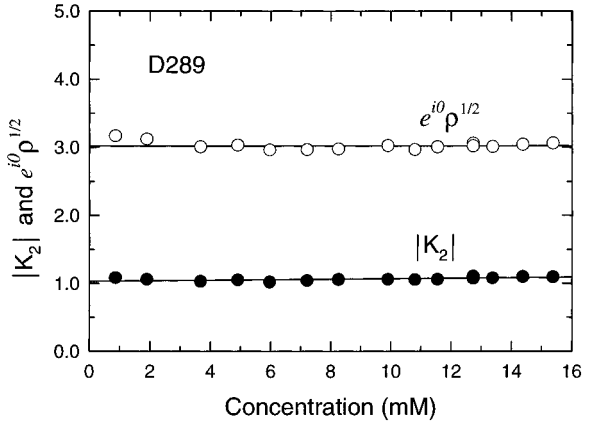

Figure 9. Change of $e^{i0}\sqrt{\rho}$ and $|K_2|$ vs the solution concentration for D289 at the CH_3CN/quartz interface. The angle of incidence was 32°.

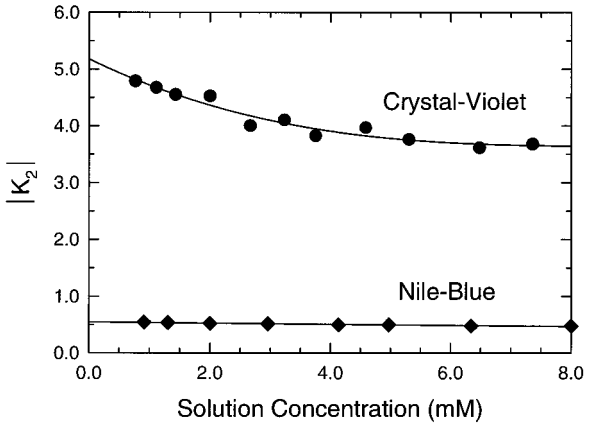

Figure 10. Change of $|K_2|$ as a function of the solution concentration for Nile Blue and Crystal Violet at the CH_3CN/quartz interface. The angle of incidence was 32°.

4.4. Change of $|K_2|$ vs Interfacial Density. Figure 9 shows the change of the values of $|K_2|$ and $e^{i0}\sqrt{\rho}$ as a function of the bulk concentration of D289. The angle of incidence at the CH_3CN/quartz interface was 32° and the interfacial density of D289 is proportional to its bulk concentration. As shown by Figure 9, the value of $|K_2|$ is also independent of the interfacial density. The average value of $|K_2|$ is about 1.06, which is very close to that obtained from the results shown in Figure 7, $K_2 = 1.04$. This result indicates that $\beta_{z'z'z'}$ is the only dominant tensor component for D289 molecules, according to section 2.7. The average tilting angle (θ) of D289 at the quartz/CH_3CN interface is about 50°.[68]

For Nile Blue and Crystal Violet, however, their behaviors are significantly different from that of D289. The results are shown in Figure 10, where the values of $|K_2|$ of these two molecules are plotted as a function of their bulk concentration. The angle of incidence at the CH_3CN/quartz interface was 32°. For Nile Blue, the value of $|K_2|$ is about 0.51 and is independent of its bulk concentration. For Crystal Violet, however, its $|K_2|$ value changes considerably with its bulk concentration and approaches 5.2 at the zero concentration limit. This may be caused by the change of the molecular orientation with the interfacial density. Thus, for both molecules we have $|\chi^{(2)}_{XXZ}/\chi^{(2)}_{ZYY}| \neq 1$. This is probably because either the two molecules have more than one dominant tensor component in their hyperpolarizibility tensor matrix $\{\beta^{(2)}_{ijk}\}$ or the dominant tensor component is not $\beta_{z'z'z'}$.

V. Conclusions

A new experimental method has been developed for the determination of the nonlinear optical tensor ratios, $|\chi^{(2)}_{ZZZ}/$

$\chi^{(2)}_{ZYY}|$ and $|\chi^{(2)}_{XXZ}/\chi^{(2)}_{ZYY}|$, for molecules at solid−liquid interfaces using transmission second-harmonic generation. The experimental results are in excellent agreement with nonlinear optical theory. For D289 molecules, $|\chi^{(2)}_{ZZZ}/\chi^{(2)}_{ZYY}| = 1.41$ and $|\chi^{(2)}_{XXZ}/\chi^{(2)}_{ZYY}| = 1.04$, while for Crystal Violet, $|\chi^{(2)}_{ZZZ}/\chi^{(2)}_{ZYY}| = 7.9$ and $|\chi^{(2)}_{XXZ}/\chi^{(2)}_{ZYY}| = 3.9$ when the bulk concentration is 4 mM. For the determination of the average molecular orientation at the interface, the following procedures are suggested:

(1) The values of $|K_2|$ at low interfacial densities should be determined according to eq 27. If $\beta_{z'z'z'}$ is the only dominant tensor component in the hyperpolarizability tensor matrix $\{\beta^{(2)}_{ijk}\}$, the value of $|K_2|$ should approach 1.0 at the low interfacial density limit.

(2) The phase angle ξ of the factor $e^{i\xi}\sqrt{\rho(\alpha_i)}$ can be determined by monitoring the change of the p-polarized SHG signal as a function of the polarization angle ϕ, according to eq 23.

(3) The value of K_1 can be determined from the change of $e^{i\xi}\sqrt{\rho(\alpha_i)}$ as a function of the angle of incidence, according to eq 28. If $\beta_{z'z'z'}$ is the only dominant tensor component in the hyperpolarizibility tensor matrix $\{\beta^{(2)}_{ijk}\}$, the orientation factor $\langle\cos\theta\rangle/\langle\cos^3\theta\rangle$ can be obtained according to eq 30.

Acknowledgment. We acknowledge with thanks the financial support for this work by the Department of Energy (through the Center for Molecular Electronics at the University of Missouri−St. Louis), the Missouri Research Board, the Research Incentive Award from the University of Missouri−St. Louis, and the Monsanto Postdoctoral Fellowship.

References and Notes

(1) Beyer, D.; Bohanon, T. M.; Knoll, W.; Ringsdorf, H. *Langmuir* **1996**, *12*, 2514.
(2) Bierbaum, K.; Grunze, M. *Langmuir* **1995**, *11*, 2143−2150.
(3) Folkers, J. P.; Laibinis, P. E.; Whitesides, G. M. *J. Phys. Chem.* **1994**, *98*, 563−571.
(4) Chaudhury, M. K.; Whitesides, G. M. *Science* **1992**, *255*, 1230−1232.
(5) Stayton, P. S.; Olinger, J. M.; Jiang, M.; Bohn, P. W.; Sligar, S. *J. Am. Chem. Soc.* **1992**, *114*, 9298−9299.
(6) Dubois, L. H.; Zegarski, B. R.; Nozzo, R. G. *J. Am. Chem. Soc.* **1990**, *112*, 570−579.
(7) Whitesides, G. M; Laibinis, P. E. *Langmuir* **1990**, *6*, 87−96.
(8) Balachander, N.; Sukenik, C. N. *Langmuir* **1990**, *6*, 1621−1627.
(9) Lee, H.; Kepley, L. J.; Hong, H. G.; Akhter, S.; Mallouk, T. E. *J. Phys. Chem.* **1988**, *92*. 2597−2601.
(10) Dubois, L. H.; Zegarski, B. R.; Nuzzo, R. G. *Proc. Natl. Acad. Sci. U.S.A.* **1987**, *84*, 4739−4742.
(11) Allara, D. L.; Nuzzo, R. G. *Langmuir* **1985**, *1*, 45−52.
(12) Sagiv, J. *J. Am. Chem. Soc.* **1980**, *102*, 92.
(13) Sneddon, D. D.; Sabel, D. M.; Gewirth, A. A. *J. Electrochem. Soc.* **1995**, *142*, 3027−3033.
(14) Ishikawa, M.; Enomoto, H.; Matsuoka, M.; Iwakura, C. *Electrochim. Acta* **1995**, *40*, 1663−1668.
(15) Sicker, D.; Hartenstein, H.; Mouats, C.; Hazard, R.; Tallec, A. *Electrochim. Acta* **1995**, *40*, 1669−1674.
(16) Schmidt, V. M.; Pastor, E. *J. Phys. Chem.* **1995**, *99*, 13247−13256.
(17) Richard, K. M.; Gewirth, A. A. *J. Phys. Chem.* **1995**, *99*, 12288−12293.
(18) Gale, R. J., Ed. *Spectroelectrochemistry*; Plemum Press: New York, 1988.
(19) Kalvoda, R., Parsons, R., Eds. *Electrochemistry in Research and Development*; Plenum Press: New York, 1985.
(20) Conway, B. E., White, R. E., Bockris, J. O'M., Eds. *Modern Aspects of Electrochemistry*; Plenum Press: New York, 1985.
(21) Bard, A. J.; Faulkner, L. R. *Electrochemical Methods: Fundamental and Application*; John Wiley & Sons, Inc.: New York, 1980.
(22) Holmes, P. J., Ed. *Electrochemistry of Semicondutors*; Academic Press: New York, 1962.
(23) Tidblad, J.; Leygraf, C. *J. Electrochem. Soc.* **1995**, *142*, 749−756.
(24) Zakipour, S.; Tidblad, J.; Leygraf, C. *J. Electrochem. Soc.* **1995**, *142*, 757−760.
(25) Kim, J.; Pyun, S. I. *Electrochim. Acta* **1995**, *40*, 1863−1870.
(26) Al-Kharafi, F. M.; Badawy, W. A. *Electrochim. Acta* **1995**, *40*, 1811−1818.
(27) Xu, Z.; Lau, S.; Bohn, P. W. *Surf. Sci.* **1993**, *296*, 57−66.
(28) Xu, Z.; Lau, S.; Bohn, P. W. *Langmuir* **1993**, *9*, 993−1000.
(29) Plakatouras, J. C.; Perlepes, S. P.; Mentzafos, D.; Terzis, A.; Bakas, T.; Papaefthymiou, V. *Polyhedron* **1992**, *11*, 2657−2672.
(30) Cruickshank, B. J.; Gewirth, A. A.; Rynders, R. M.; Alkire, R. C. *J. Electrochem. Soc.* **1992**, *139*, 2829−2832.
(31) Xue, G.; Dong J.; Wu, P. *J. Polym. Sci.* **1992**, *30*, 1097−1102.
(32) Thomas, R. R.; Brusic, V. A.; Rush, B. M. *J. Electrochem. Soc.* **1992**, *139*, 678−685.
(33) Aramaki, K.; Kiuchi, T.; Sumiyoshi, T.; Hishhara, H. *Corros. Sci.* **1991**, *32*, 593−607.
(34) Brusic. V.; Frisch, M. A.; Eldridge, B. N.; Novak, F. P.; Kaufman, F. B.; Rush, B. M.; Frankel, G. S. *J. Electrochem. Soc.* **1991**, *138*, 2253−2259.
(35) Bhattacharya, R. N.; Fernandez, A. M.; Contreras, M. A.; Keane, J.; Tennant, A.L.; Ramanathan, K.; Tuttle, J. R.; Noufi, R. N.; Hermann, A. M. *J. Electrochem. Soc.* **1996**, *143*, 845.
(36) Thouin, L.; Vedel, J. *J. Electrochem. Soc.* **1995**, *142*, 2996−3000.
(37) Awada, M.; Strojek, J. W.; Swain, G. M. *J. Electrochem. Soc.* **1995**, *142*, L42−L45.
(38) Moller, F.; Magnussen, O. M.; Behm, R. J. *Electrochim. Acta* **1995**, *40*, 1259−1266.
(39) Ogaki, K.; Itaya, K. *Electrochim. Acta* **1995**, *40*, 1249−1258.
(40) Gorman, C. B.; Biebuyck, H. A.; Whitesides, G. M. *Langmuir* **1995**, *11*, 2242−2246.
(41) Carnal, D.; Oden, P. I.; Müller, U.; Schmidt, E.; Siegenthaler, H. *Electrochim. Acta* **1995**, *40*, 1223−1226.
(42) Gofer, Y.; Barbour, R.; Luo, Y.; Tryk, D.; Scherson, D. A.; Jayne, J.; Chottiner, G. *J. Phys. Chem.* **1995**, *99*, 11739−11741.
(43) Dorsey, J. G.; Cooper W. T.; Siles, R. A.; Foley, J. P.; Barth, H. G. *Anal. Chem.* **1996**, *68*, 515R.
(44) Claire, R. L. St., III. *Anal. Chem.* **1996**, *68*, 569R.
(45) Corn, R. M.; Higgins, D. A. *Chem. Rev.* **1994**, *94*, 107−125.
(46) Vogel, V.; Shen, Y. R. *Annu. Rev. Mater. Sci.* **1991**, *21*, 515−534.
(47) Shen, Y. R. *Nature* **1989**, *337*, 519−525.
(48) Richmond, G. L.; Robinson, J. M.; Shannon, V. L. *Prog. Surf. Sci.* **1988**, *28*, 1−70.
(49) Robinson, J. M.; Rojhantalab, H. M.; Shannon, V. L.; Richmond, G. L. *Pure Appl. Chem.* **1987**, *59*, 1263−1268.
(50) Heinz, T. F.; Tom, H. W. K.; Shen, Y. R. *Laser Focus* **1983**, *May*, 101−108.
(51) Lundquist, P. M.; Yitzchaik, S.; Zhang, T. G.; Kanis, D. R; Ratner, M. A.; Marks, T. J.; Wong, G. K. *Appl. Phys. Lett.* **1994**, *64*, 2194−2196.
(52) Higgins, D. A.; Abrams, M. B.; Byerly, S. K.; Corn, R. M. *Langmuir* **1992**, *8*, 1994−2000.
(53) Gordon, F. W.; Cresswell, S. A.; Steehler, J. K. *Langmuir* **1989**, *5*, 286−288.
(54) Heinz, T. F.; Chen, C. K.; Ricard, D.; Shen, Y. R. *Phys. Rev. Lett.* **1982**, *48*, 478−481.
(55) At air−solid interfaces, the light-induced degradation is mainly caused by multiple photon dissociation. At solid−liquid interfaces, however, the energy transfer by collision with solvent molecules will significantly reduce the possibility of this process.
(56) Shen, Y. R. *The Principle of Nonlinear Optics*; Wiley: New York, 1985.
(57) Bloembergen, N.; Pershan, P. S. *Phys. Rev.* **1962**, *128*, 606.
(58) The refractive index of fused silica changes from 1.45 at 1000 nm to 1.50 at 250 nm. Melles Griot, *Optical Guide*, 1995/1996.
(59) Guyot-Sionnest, P.; Chen, W.; Shen, Y. R. *Phys. Rev. B* **1986**, *33*, 8254.
(60) Dluhy, R. A. *J. Phys. Chem.* **1986**, *90*, 1373.
(61) $I = \epsilon_0\epsilon_t(c/n)\langle E^2\rangle = \epsilon_0 cn\langle E^2\rangle$, in which $\epsilon_r = n^2$ is the relative dielectric constant.
(62) In general, the terms in brackets in eq 21 are complex numbers.[63]
(63) Campbell, D. J.; Lynch, M. L.; Corn, R. M. *Langmuir* **1990**, *6*, 1656.
(64) Under our experimental conditions using quartz as the substrate and using the optically transparent solvent CH_3CN, all local field factors (L_X, L_Y, L_Z) are real.
(65) When the condition specified by eq 7 can be assumed,

$$|K_1| = \left|\frac{\chi^{(2)}_{ZZZ}}{\chi^{(2)}_{ZYY}}\right| = \frac{2\langle\cos^3\theta\rangle}{\langle\cos\theta\sin^2\theta\rangle} = \frac{2\langle\cos^3\theta\rangle}{\langle\cos\theta\rangle - \langle\cos^3\theta\rangle} = 2\left[\frac{\langle\cos\theta\rangle}{\langle\cos^3\theta\rangle} - 1\right]^{-1}$$

(66) Li, D.-Q.; Ratner, M. A.; Marks, T. J.; Zhang, C. H.; Yang, J.; Wong, G.K. *J. Am. Chem. Soc.* **1990**, *112*, 7389.
(67) Dakkar, A. K.; Yitzchaik, S.; Roscoe, S. B.; Kubota, F.; Lin, W.; Wong, G. K. *Langmuir* **1993**, *9*, 388.
(68) Here, we assume that the angular distribution of D289 molecules at the interface is a δ-function.